ANALYSIS OF VORTEX PACKETS AND REYNOLDS STRESS IN A TURBULENT BOUNDARY LAYER

E K Longmire, B Ganapathisubramani & I Marusic
Department of Aerospace Engineering and Mechanics,
University of Minnesota
107 Akerman Hall, 110 Union Street SE, Minneapolis, MN 55455, USA
ellen@aem.umn.edu, bugs@aem.umn.edu, marusic@aem.umn.edu

ABSTRACT

Sets of stereo PIV measurements were obtained in streamwise-spanwise planes of a turbulent boundary layer with $Re_\tau = 1060$. Two-point spatial correlations obtained from fields in the logarithmic region revealed that both streamwise-streamwise (R_{uu}) and streamwise-wall-normal (R_{uw}) correlations were significant for streamwise displacements of more than 1500 wall units. Zero crossing data for the streamwise fluctuating component u revealed that streamwise strips between zero crossings of 1500 wall units or longer occurred more frequently for negative u than positive u. This result suggested that the long streamwise correlations in R_{uu} are dominated by slower streamwise structures. Additional analysis of R_{ww} correlations suggested that the long slow-moving streamwise structures contain discrete zones of strong upwash over extended streamwise distances as might occur within packets of angled hairpin vortices. At a wall-normal location outside of the log region ($z/\delta = 0.5$), the correlations were shorter in the streamwise direction and broader in the spanwise direction. All of the correlation results are consistent with earlier studies (Ganapathisubramani *et al*, 2003) in which a feature detection algorithm identified packets of hairpins in the log region but not in the outer region.

INTRODUCTION

In the current study, we attempt to examine the structure of the logarithmic region of the boundary layer and its relation to the Reynolds shear stress. In this region, both experimental and numerical studies have postulated and documented the existence of hairpin-like vortices inclined at an angle to the free stream (see, for example, Head and Bandyopadhyay, 1981 and Robinson, 1991) that are thought to be responsible for the generation of bursting and ejection events in which slow moving fluid is lifted away from the wall. These events are thought to be strong contributors to the Reynolds stress within the boundary layer and consequently to surface drag. More recently, Adrian *et al* (2000) and Tomkins and Adrian (2002) have documented the existence of 'vortex packets' in turbulent boundary layers by performing planar PIV measurements in streamwise-wall-normal and streamwise-spanwise flow planes respectively. The experimental results corresponded well with three-dimensional simulations of Zhou *et al* (1999) examining the development and propagation of such packets. The existence of vortices organized within packets also helps explain the long tails on streamwise velocity autocorrelations within the boundary layer (see Townsend, 1976).

In this paper, an experimental investigation is presented on the structure of the turbulent boundary layer in the logarithmic region (taken here nominally as $z^+ = zU_\tau/\nu > 70$ and $z/\delta < 0.15$, where z is the wall normal location, U_τ is the skin friction velocity and ν is the kinematic viscosity) and beyond. Stereoscopic particle image velocimetry was used to measure all three velocity components in streamwise-spanwise planes ($x-y$ planes) of a turbulent boundary layer at $Re_\tau = 1060$ ($Re_\tau = \delta U_\tau/\nu$, where δ is the boundary layer thickness). Measurements were acquired and analyzed at several wall-normal locations. In previous work (Ganapathisubramani *et al.*, 2003), we used a feature detection algorithm to examine vortical structures and packets occurring in instantaneous velocity fields. The goal of the current study is to present ensemble-averaged statistics based on the same velocity fields to provide additional evidence for the dominant structural features in the flow.

EXPERIMENTAL FACILITY AND METHODS

The experiments were performed in a suction type boundary layer wind tunnel. Measurement planes were located 3.3 m downstream of a trip wire in a zero-pressure-gradient flow with freestream velocity $U_\infty = 5.9$ m s^{-1}. The flow was seeded with olive oil particles and illuminated by pulsed sheets from two Nd:YAG lasers (Big Sky CFR200, 120 mJ) directed through one side window and oriented parallel with the bottom wall of the tunnel. Sets of digital images were captured by two Kodak Megaplus CCD cameras (1024 × 1024 pixels) at $z^+ = 530$, ($z/\delta = 0.5$) and by TSI Powerview 2048 × 2048 pixel resolution cameras at $z^+ = 92$ and $z^+ = 150$. For all derived quantities, the interrogation spot size used was 16×16 pixels ($\sim$ 20×20 wall units) with 50% overlap. Hence the spacing between adjacent velocity vectors in either direction is 10 wall units ($\sim$ 0.65 mm).

Spatial velocity derivatives were computed on the grid of the vector field using a second order central difference method within the domain and a first order method at the boundaries. Vortex cores were identified by computing the swirl strength (λ_{ci}) which is the imaginary part of the eigenvalue of the two dimensional velocity gradient tensor. In the following discussion, fluctuating velocities (velocity differences from the mean) are denoted by u, v, and w for the streamwise, spanwise, and wall-normal components respectively.

To detect hairpin vortices and hairpin packets in the stereo PIV fields, we developed a feature extraction algorithm which is explained in detail in Ganapathisubramani *et al.* (2003). The algorithm searches for neighboring streamwise strips of negative and positive vorticity, where negative vorticity is clockwise rotation when viewing a field with streamwise velocity moving from left to right. This vorticity

arrangement was chosen to fit the pattern displayed by the legs of a hairpin vortex. Since angled hairpins are expected to generate large values of instantaneous Reynolds shear stress ($-uw^+ = -uw/{U_\tau}^2$), the algorithm also searches for locations where $-uw^+$ is greater than $2\sigma_{-uw}{}^+$ where $\sigma_{-uw}{}^+$ is the r.m.s. of $-uw^+$. Locations with large $-uw^+$ falling between the strips of vorticity are then used as seed points in a region-growing algorithm. This algorithm identifies connected regions of points with streamwise velocity lying within local thresholds such that the final coherent region is a patch of uniform momentum. The criterion for uniform momentum attempts to satisfy the idea that hairpins traveling in a packet convect at a relatively uniform speed.

To quantify spatial coherence within the homogeneous velocity fields acquired, two point correlations were calculated. An overview of the notation used to describe two-point correlations follows. The components of separation between any two points in space are denoted by $(\Delta x, \Delta y)$ in the two in-plane directions. Then the two-point correlation coefficient between any two quantities (A and B, where A and B can be any turbulent fluctuating quantity) R_{AB} is defined as,

$$R_{AB}(\Delta x, \Delta y) = \frac{\overline{A(x,y)B(x+\Delta x, y+\Delta y)}}{\sigma_A \sigma_B} \qquad (1)$$

where, σ_A and σ_B are the standard deviation of A and B respectively. The overline notation represents an ensemble average over multiple realizations. The number of velocity fields used to compute statistics were 300, 300 and 750 at $z^+ = 92$, $z^+ = 150$ and $z^+ = 530$ respectively.

In addition to computing correlation functions, we also investigated the probability density of the streamwise distance between zero crossings in u. (A zero crossing is defined as the location at which a fluctuating quantity changes sign). We computed the probability density of a quantity versus streamwise length (length is the distance over which the quantity remains above zero or below zero). This is similar to the zero crossing events characterized by Kailasnath and Sreenivasan (1993). However, in the present work we have distinguished between a quantity crossing zero from positive to negative and vice versa. This will give information on distance over which a quantity remains either above or below zero.

RESULTS

An example of a vector field at $z^+ = 150$, nominally in the logarithmic region, is given in Figure 1(a). The plot shows in-plane velocity vectors with the local mean velocity ($0.65U_\infty$) subtracted as well as gray-scale contours of the Reynolds stress. The regions outlined in black were identified by the feature detection algorithm as hairpin packets. Note that the identified packets also include single hairpin vortices that satisfy the detection criteria. It can be seen from the plot that the packets contain small zones of large Reynolds stress, but they also contain significant areas of low Reynolds stress. Also, an area of strong $-uw$ located at (x,y) = (1500, 2000) is not contained within a packet, most likely because it has $u > 0$. (The vorticity pattern in the feature detection algorithm dictates that $u < 0$).

Figure 1(b) shows a zoomed in view of the packet in the upper right-hand corner of Figure 1(a). In this case,

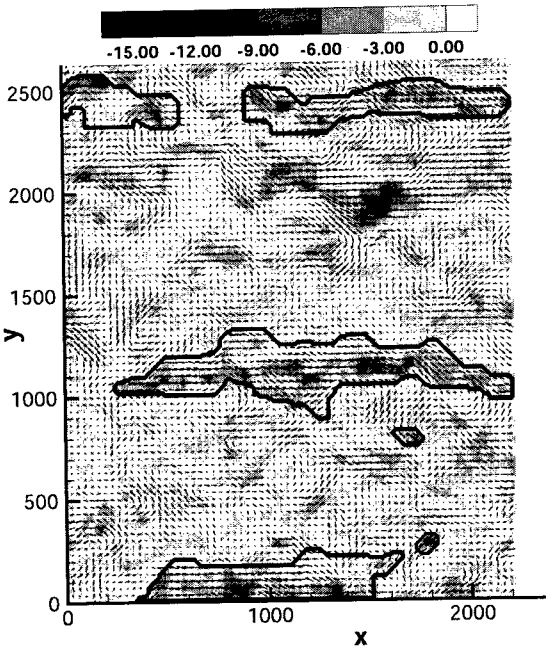

(a)

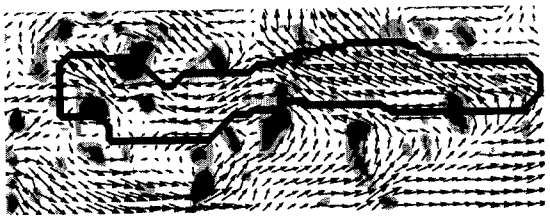

(b)

Figure 1: (a) Reynolds shear stress at $z^+ = 150$, (b) Swirl strength contours at $z^+ = 150$

contours of swirl are plotted in order to demonstrate that the packet is bounded by a number of distinct cores. This plot as well as additional plots of swirl magnitude indicate that the longer packets exhibit cross sections of multiple pairs of cores associated with individual hairpins. Typically, the hairpins observed at $z^+ = 92$ and 150 have two legs crossing the measurement plane. The legs may be either aligned or somewhat offset in streamwise location.

A detailed examination of many Reynolds stress plots shows also that the individual hairpins must be angled, as they generate intermittent regions of intense Reynolds stress. A key result from an investigation of many fields at two heights ($z^+ = 92$ and 150) was that the identified packets occupied only 4-5% of the total spanwise area examined yet contributed 25-28% of the total shear stress $\overline{-uw}$ (See Ganapathisubramani *et al*, 2003).

Figure 2 shows the joint probability density of u and w for all points measured at $z^+ = 92$. The set of all values shows the skew toward negative values of uw observed in previous hot-wire studies. The set of possible seed points for the algorithm is marked by solid gray contours, and the set of all points within the zones identified as packets is marked by black contours. The contour locations show clearly that the packets contain some but not all of the largest values of $-uw$. In addition, the packets contain mostly positive but also some negative wall-normal velocities. Thus, the relatively large Reynolds stress contribution of the packets seems even more significant as it would be even larger if the

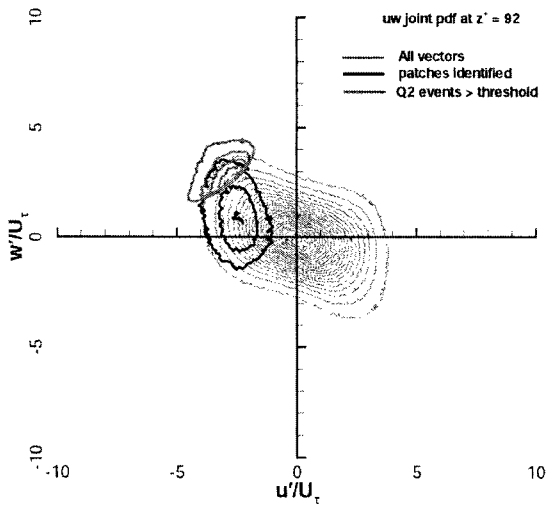

Figure 2: u and w joint number density at $z^+ = 92$

positive uw values were not included. Note also that, by design, no Q4 events ($u > 0, w < 0$) are included within the packets.

Figures 3(a) and 3(b) show the two point autocorrelation R_{uu} at $z^+ = 92$ and $z^+ = 530$ respectively. It is quite clear from the first plot that there is significant spatial coherence in the streamwise direction in the log region ($z^+ = 92$) such that the correlation coefficient extends greater than 1500 wall units (1.5δ). The equivalent plot at $z^+ = 530$ (0.5δ) is much shorter, extending a distance of only 0.6δ. Additional correlation plots from intermediate planes suggest that the extent of the streamwise coherence drops off significantly beyond the log layer. The reduced streamwise coherence was also observable in vector plots beginning at $z^+ = 192$, which typically contained evidence of larger individual vortex cores, upwash and downwash regions, and possibly cross sections of individual hairpin heads (See Longmire *et al.*, 2001). Furthermore, the feature detection algorithm described earlier did not identify any long packets when applied at $z^+ = 530$.

At $z^+ = 92$, the width of the positive correlation region in the spanwise direction is about 400 wall units, with a zero crossing at $\Delta y^+ = 200$. At $z^+ = 530$, however, the positive correlation is wider with the zero crossing occurring at $\Delta y^+ = 400$. The spanwise results demonstrate that typical flow structures increase in width with increasing wall-normal distance. At $z^+ = 92$, the negative correlation outside of the positive correlation supports the idea of adjacent low and high speed streaks extending in the streamwise direction. This result is consistent with the findings of other work in the literature(see Townsend, 1976).

The long streamwise coherence at $z^+ = 92$ could be caused either by long streaks of negative u as observed in the packet structures or by long streaks of positive u which are sometimes observed on either side of the packets. In order to investigate the relative contributions, lines of vectors in the streamwise direction were examined for the streamwise length between zero crossings. In this case, a zero crossing occurs when the fluctuating component u changes sign. Separate probability density functions were generated for lengths of positive and negative u between zero crossings. The normalized difference between these functions is plotted in Figure 4 where a negative value in the ordinate indicates that strips of negative u occur more frequently than strips of positive u for a given length value Δx^+. The plot

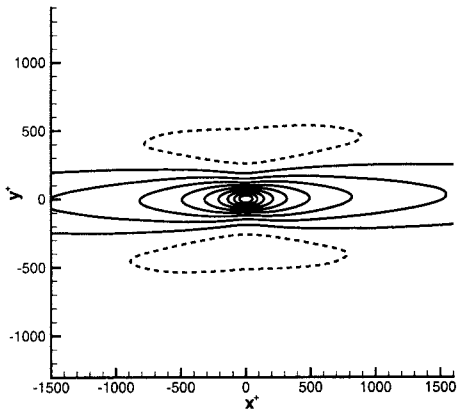

(a)

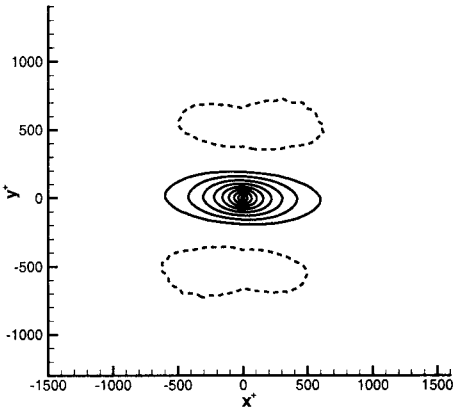

(b)

Figure 3: (a) R_{uu} correlation at $z^+ = 92$, (b) R_{uu} correlation at $z^+ = 530$. The contour levels for R_{uu} range from -0.1 to 1.0 with spacing of 0.1. Zero contours are not shown.

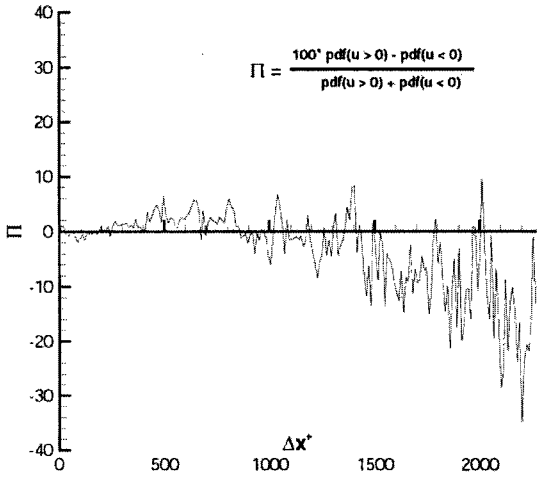

Figure 4: Difference between zero crossings of positive and negative u at $z^+ = 92$. The abscissa Δx^+ gives the streamwise length over which the quantity remained above or below zero

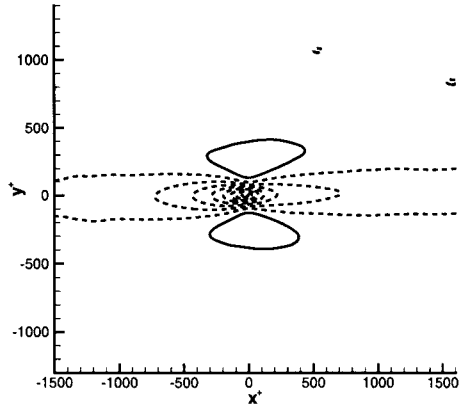

(a)

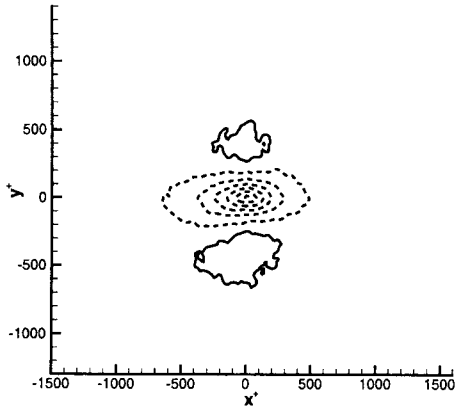

(b)

Figure 5: (*a*) R_{uw} correlation at $z^+ = 92$, (*b*) R_{uw} correlation at $z^+ = 530$. The contour levels for R_{uw} range from -0.05 to 0.5 with spacing of 0.05. Zero contours are not shown.

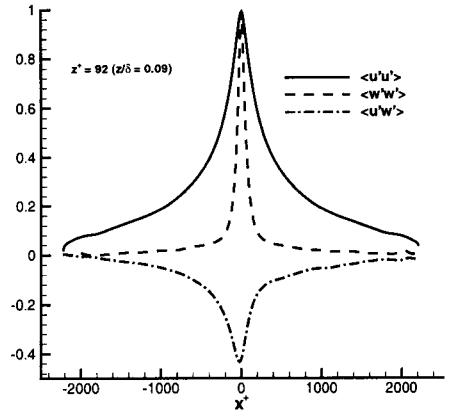

(a)

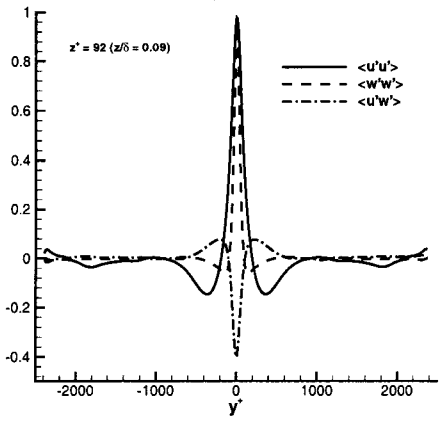

(b)

Figure 6: R_{uu}, R_{ww} and R_{uw} correlations in (*a*) streamwise and (*b*) spanwise directions along the centerline at $z^+ = 92$

shows that short streamwise strips of negative and positive u occur with approximately equal probability. However, for streamwise strips between zero crossings longer than 1500 wall units, those with negative u occur significantly more frequently than those with positive u. This result suggests that the long streamwise correlations in R_{uu} are dominated by slower streamwise structures such as those within vortex packets.

The primary advantage of performing Stereo PIV experiments is the availability of all three velocity components. Hence, we can compute all possible velocity auto- and cross-correlations over the streamwise-spanwise plane. In the following paragraphs, we focus on R_{uw}, the streamwise-wall-normal correlation because of its relation to the dominant component of Reynolds shear stress. Figures 5(a) and 5(b) show the R_{uw} correlation at $z^+ = 92$ and 530 respectively. As with uu, the uw correlation extends over a long streamwise distance at $z^+ = 92$, but the correlation values are negative for $\Delta y^+ = 0$. The maximum magnitude of R_{uw} is about 0.42. Given the dominance of slow moving fluid in long correlations shown by Figure 4, the negative values suggest that slow moving fluid is associated with upwash (flow away from the wall) over long streamwise distances. Further away from the wall at $z^+ = 530$, the uw correlation decreases in length and increases in width similar to the behavior of uu.

The maximum magnitude at $z^+ = 530$ is about 0.4 which is close to the correlation values found by Tritton (1967) in his hot-wire experiments. One other point worth observing is the zero crossing of the R_{uw} correlation in the spanwise direction. The presence of the zero crossing suggests that slow moving fluid is correlated with flow away from the wall at a distance of about 200 wall units on either side. This observation is in accordance with the inclined hairpin vortex theory as proposed by Theodorsen (1952) which was later refined by other researchers to explain the dynamics of turbulent boundary layers (for example, see Perry and Chong, 1982 and Perry and Marusic, 1995).

Figure 6 gives the R_{uu}, R_{ww} and R_{uw} correlations extracted along the centerline in the streamwise and spanwise directions at $z^+ = 92$. First, in Figure 6(a), note that the R_{ww} correlation drops very sharply when $\Delta x^+ \leq 100$ suggesting that the streamwise coherence in w is typically quite short. On the other hand, the peak in R_{uw} drops off

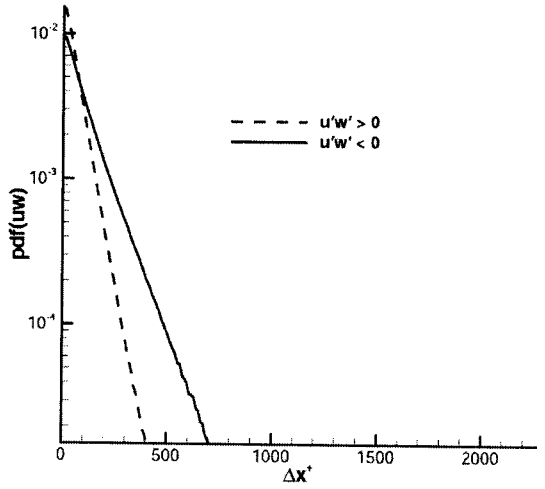

Figure 7: Distance between zero crossings of positive and negative uw at $z^+ = 92$. The abscissa Δx^+ gives the streamwise length over which the quantity remained above or below zero

more slowly, and the correlation has significant magnitude over a streamwise distance of order 1400 wall units. The R_{uu} correlation extends beyond the streamwise range examined. Taken together, these results suggest that slow moving fluid is correlated with discrete zones of upwash over an extended streamwise distance both upstream and downstream as might occur with packets of hairpin vortices moving with similar convection speeds. Each hairpin ejects fluid away from the wall (thereby making correlation of R_{ww} compact and short) between the legs as suggested by Adrian, Meinhart and Tomkins (2000).

Similar to the present results, Tomkins and Adrian (2002) found that a conditional eddy (conditioned on slow moving zones) in the streamwise-spanwise plane bore a striking resemblance to a hairpin vortex signature. They also found that the spanwise width of the structure and the separation between the legs increased away from the wall which is analogous to the increase in the spanwise extent of the R_{uu} correlations presented here. In figure 6(b), the R_{ww} correlation is narrower in the spanwise direction than R_{uu}, and its negative lobe is weaker suggesting in general that coherence in w is narrower than in u. In any case, the presence of negative lobes in R_{ww} suggest that upwash locations are frequently bounded by downwash as would occur in hairpin vortices where an ejection between angled legs would be accompanied by inward sweeps outside of the legs.

A zero crossing analysis was also performed on the uw product at $z^+ = 92$. Similar to the case of u, separate probability density functions were determined for the length of streamwise strips between zero crossings for both $uw < 0$ and $uw > 0$. The resulting pdf's are plotted in Figure 7. These distributions are narrower than those based on u generated for Figure 4, which can be expected based on the correlation plots. The distribution of $uw < 0$ is broader than that of $uw > 0$ indicating that $uw < 0$ is associated with slightly longer structures. This result might be explained by the argument that $uw < 0$ events derive naturally from angled eddies generating upwash and downwash while $uw > 0$ events are more stochastic. This is an area we will examine more closely in the future. When $uw < 0$ is broken down into separate zero crossing length distributions for Q2 ($u < 0$) and Q4 ($u > 0$), no significant difference was observable

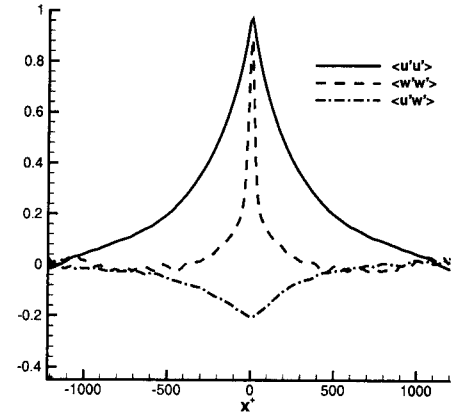

(a)

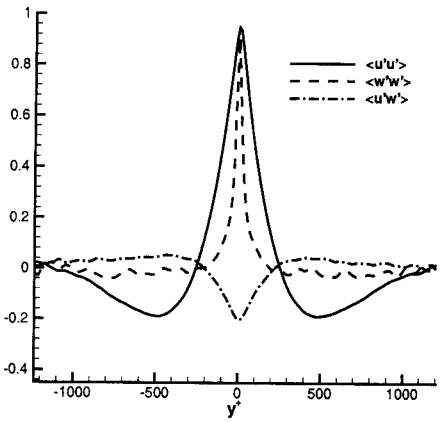

(b)

Figure 8: R_{uu}, R_{ww} and R_{uw} correlations in (a) streamwise and (b) spanwise directions along the centerline at $z^+ = 530$

(and therefore the separate distributions are not shown in the plot).

Finally, for completeness we show the line plots extracted from the zero axes of the R_{uu}, R_{ww} and R_{uw} correlations at $z^+ = 530$ in Figure 8. The streamwise and spanwise axes plotted in Figures 8(a) and 8(b) extend to shorter distances than in Figure 6 because the measurements at $z^+ = 530$ covered a smaller field of view. In Figure 8(a), note that the shape of R_{ww} in the streamwise direction is quite similar to that at $z^+ = 92$. In the spanwise direction, however, R_{ww} is slightly broader than at $z^+ = 92$ which is consistent with the trend for R_{uu} and R_{uw} seen also in Figure 5(b).

CONCLUSIONS

Statistical analysis of homogeneous streamwise-spanwise planes in the log region of a turbulent boundary layer suggests that long narrow low speed zones contain intermittent zones of upwash over their length. This picture is consistent with the idea that packets of hairpin vortices give rise to the long streamwise coherence previously found by point measurement techniques. Shorter streamwise correlations in planes further from the wall suggest that many of the hairpin heads do not extend beyond this region. These

results are consistent with an earlier attached-eddy modeling study by Marusic (2001). The kinematic state of the boundary layer was modeled by a statistical ensemble of hairpin-shaped structures distributed across a range of length and velocity scales with varying population density across the length scales. The study showed that, for positions in the log region, a packet of hairpins was needed in order for the correlations to agree with experiments. However, this spatial coherence was not needed for the outer part of the boundary layer beyond the log region where adequate results were obtained with single uncorrelated hairpin vortices. The correlation results are also consistent with our related work examining instantaneous Stereo PIV fields for packet-like signatures (Ganapathisubramani *et al*, 2003).

ACKNOWLEDGMENTS

The authors gratefully acknowledge support from the National Science Foundation through Grants ACI-9982274 and CTS-9983933.

REFERENCES

Adrian, R. J., Meinhart, C. D. and Tomkins, C. D. 2000, "Vortex organization in the outer region of the turbulent boundary layer", *J. Fluid Mech.*, Vol. 422, pp 1–53.

Ganapathisubramani, B., Longmire, E. K. and Marusic, I. 2003, "Characteristics of vortex packets in turbulent boundary layers", *J. Fluid Mech.* Vol. 478, pp 35–46.

Head, M. R. and Bandyopadhyay, P. 1981, "New aspects of turbulent boundary-layer structure", *J. Fluid Mech.* Vol. 107, pp 297–337.

Kailasnath, P. and Sreenivasan, K. R., 1993, "Zero crossings of velocity fluctuations in turbulent boundary layers", *Phys. Fluids*, Vol. 5(11), pp 2879–2885

Longmire, E. K., Ganapathisubramani, B. and Marusic, I., 2001, "Structure identification and analysis in turbulent boundary layers by stereo PIV", *In Proc. 4th International symposium on Particle Image Velocimetry, Sept. 17-19 . Gottingen, Germany.*

Marusic, I. 2001, "On the role of large-scale structures in wall turbulence", *Phys. Fluids*, Vol. 13(3), pp 735–743.

Perry, A. E. and Chong, M. S., 1982, "On the mechanism of wall turbulence", *J. Fluid Mech.*, Vol. 119, pp 173–217

Perry, A. E and Marusic, I., 1995, "A wall wake model for the turbulence structure of boundary layers. Part 1. Extension of the attached eddy hypothesis", *J. Fluid Mech.*, Vol 298, pp 289–407

Robinson, S. K. 1991, "Coherent motions in turbulent boundary layers", *Annu. Rev. Fluid Mech.* Vol. 23, pp 601–639.

Theodorsen, T. 1952, "Mechanism of turbulence", *In Proc. Second Midwestern Conference on Fluid Mechanics, Mar. 17-19 Ohio state University, Columbus, Ohio.*

Tomkins, C. D. and Adrian, R. J. 2002, "Spanwise structure and scale growth in turbulent boundary layers", *TAM Reports, University of Illinois at Urbana-Champaign* # 1006.

Townsend, A. A. 1976, "The Structure of Turbulent Shear Flow", *Cambridge University Press.*

Tritton, D. J., 1967 "Some new correlation measurements in a turbulent boundary layer", *J. Fluid Mech.*, Vol. 28, pp 439

Zhou, J., Adrian, R. J., Balachandar, S. and Kendall, T. M. 1999, "Mechanisms for generating coherent packets of hairpin vortices in channel flow" *J. Fluid Mech.* Vol. 387, pp 353–396.